

Multi-objective Generative Design of Three-Dimensional Composite Materials

Zhengyang Zhang^{1†}, Han Fang^{1†}, Zhao Xu², Jiajie Lv³, Yao Shen⁴ and Yanming Wang^{1*}

¹University of Michigan-Shanghai Jiao Tong University Joint Institute, Shanghai Jiao Tong University, Shanghai, 200240, China.

²Key Laboratory of Space Utilization, Technology and Engineering Center for Space Utilization, Chinese Academy of Sciences, Beijing, 100094, China.

³School of Materials Science and Engineering, Jilin University, Changchun, 130012, China.

⁴School of Materials and Engineering, Shanghai Jiao Tong University, Shanghai, 200240, China.

*Corresponding author(s). E-mail(s): yanming.wang@stju.edu.cn;
Contributing authors: zhengyangzhang@stju.edu.cn;
han.fang@sjtu.edu.cn; xuzhao@csu.ac.cn; jiajie.lv@gmail.com;
yaoshen@sjtu.edu.cn;

[†]These authors contributed equally to this work.

Abstract

Composite materials with 3D architectures are desirable in a variety of applications for the capability of tailoring their properties to meet multiple functional requirements. By the arrangement of materials' internal components, structure design is of great significance in tuning the properties of the composites. However, most of the composite structures are proposed by empirical designs following existing patterns. Hindered by the complexity of 3D structures, it is hard to extract customized structures with multiple desired properties from large design space. Here we report a multi-objective driven Wasserstein generative adversarial

network (MDWGAN) to implement inverse designs of 3D composite structures according to given geometrical, structural and mechanical requirements. Our framework consists a GAN based network which generates 3D composite structures possessing with similar geometrical and structural features to the target dataset. Besides, multiple objectives are introduced to our framework for the control of mechanical property and isotropy of the composites. Real time calculation of the properties in training iterations is achieved by an accurate surrogate model. We constructed a small and concise dataset to illustrate our framework. With multiple objectives combined by their weight, and the 3D-GAN act as a soft constraint, our framework is proved to be capable of tuning the properties of the generated composites in multiple aspects, while keeping the selected features of different kinds of structures. The feasibility on small dataset and potential scalability on objectives of other properties make our work a novel, effective approach to provide fast, experience free composite structure designs for various functional materials.

Keywords: Composite Material; Composite Structures; Generative Design; 3D Wasserstein Generative Adversarial Network; Multi-Objective.

Introduction

Composites have been widely used in aerospace[1], biomedicine[2, 3] and energy-related[4] applications for their advantages in mechanical[5, 6], thermal[7, 8], electronic[4], impact resistance[9] and damage tolerance [10, 11]properties. In recent decades, the development of architected-materials[12, 13] and novel manufacturing techniques[14] such as additive manufacturing[15, 16] facilitates a precise control of architectures and micro-structures of constituent phases in composite materials. Composite materials with various internal structures are manufactured to tune the overall performance for their functional requirements. Thus, to provide guidelines for composite structure design and manufacturing, the structure-property relationship of the composites have become a research hot spot. The mechanical properties of structures such as regular lattices reinforced (including simple cubic, body-centered cubic, face-centered cubic and various auxetic

structures)[10, 17, 11, 18, 19, 20, 21], stochastic fibre networks reinforced (i.e. random fibre networks and Voronoi fibre networks)[16, 22, 23], and triply periodic minimal surfaces reinforced composites (categorized as Spinodal Shell/Solid, Schwarz Primitive, etc.)[24, 25, 26, 27, 28] have been tuned by adjusting their structural designs.

However, the majority of studies focused on a specific type of composite structure by empirical or trial-and-error methods. A structural design space much larger than currently popular composite structures remains unexplored. It is still hindered by the structural diversity and complexity of 3D composite structures to explore the huge structural design space for proposing new structures. Modern machine learning methods[29, 30, 31, 32, 33, 34] are considered as promising approaches to fulfill this kind of objectives and have been used to help the property prediction and design of various materials including polymer membranes[35], alloys[36, 37], and solid-state electrolytes[38]. In terms of composites, machine learning models (mainly convolutional neural network, CNN) showed both good accuracy (95%) and efficiency (250 times faster than finite element method, FEM) in predicting mechanical properties of 2D structures and pinpointed high performers for toughness or strength[39]. Cecen et. al.[31] and Liu et. al.[29] built structure-property regression models for composites by M5 model tree and CNN algorithms. Inputting 2D composite structures as images to machine learning models, thermal conductivity predictions of composites were also achieved via support vector regression (SVR), Gaussian process regression (GPR) and CNN[40].

Among the machine learning approaches, generative models have been proved promising to assist the inverse design of compositions[41], molecular configurations[42, 43, 44, 45, 46] as well as macro structures. For example, variational autoencoders (VAE) were introduced to provide optimal combinations

of multiple representative structures of two-dimensional composite materials with the largest elastic properties[30]. Mao et. al. utilized generative adversarial networks (GAN) to generate two-dimensional porous isotropic structures with various porosities and high Young's moduli[47]. However, those works about structures are mostly based on 2D structures, or only generate similar structures with no other design objectives involved[48]. The generative design under physics-based objectives of 3D composite structures still haven't been achieved.

In this paper, we aim to develop a multi-objective driven, three-dimensional generative design framework for composite structures by integrating physics based controls into data driven methods. Wasserstein Generative Adversarial Network (WGAN) is extended to 3D space as a soft constraint to ensure the structural features similarity between generated structures and those in the training dataset, while 3D ResNet based surrogate model is trained to give real-time evaluations of their elastic characters including Young's moduli and isotropy. We introduce multiple design objectives including structural symmetry, elastic moduli, and mechanical isotropy fulfilled by mechanics based loss functions. We construct relatively small and concise dataset by automated finite element (FE) calculations of composite structures. Our generated structures demonstrate the capability of our framework to tuned performance for composite materials to meet given objectives while keeping targeted geometrical and structural features.

Results

3D MDWGAN Framework

Our 3D Multi-objective Driven Wasserstein GAN (MDWGAN) framework (Figure 1a) mainly consists of two key components: a generative network with

multiple objectives, and a pre-trained 3D surrogate model to give evaluations for the objectives. Based on the the idea of Wasserstein GAN (WGAN)[49] and its modified version Wasserstein GAN-Gradient Penalty (WGAN-GP)[50], we developed an extended 3D-WGAN-GP network (including 3D generator and 3D discriminator) to keep the structural similarity of generated structures and structures in the dataset. Furthermore, multiple objectives are introduced and combined with the original WGAN-GP loss function to control the properties of the composites. A surrogate model is introduced to calculate the properties real time in training iterations.

Objective functions

In our model, we mainly focus on three parts of objectives: \mathcal{O}_{sim} , \mathcal{O}_{lg} and \mathcal{O}_{iso} . Each objectives gives a direction for the 3D-based generator to optimize and they are combined with different weights to achieve desired performances.

\mathcal{O}_{sim} denotes the objective that imitates the data from the original training set. This objective can be also regarded as a soft constraint embedded in MDWGAN. Since we aim at generating new structure designs, we do not intended to add hard constraints to limit the volume fraction of strong phase V_r of the composite, the geometrical symmetry, or the pattern of constituent material construction. Instead, we rely on a 3D, GAN-like network. That is, the 3D discriminator will restrain the behaviour of the 3D generator by distinguishing the structures produced by 3D-based generator from the training data, based on their similarity. Note that this is a probabilistic prediction of reinforcement phase locations given by not only one parameter such as the fraction of strong phase, but also partially inherits geometrical and structural features of the training data.

\mathcal{O}_{lg} describes the objective that the model has a tendency to generate structures with higher average moduli. \mathcal{O}_{iso} denotes the isometric moduli objective,

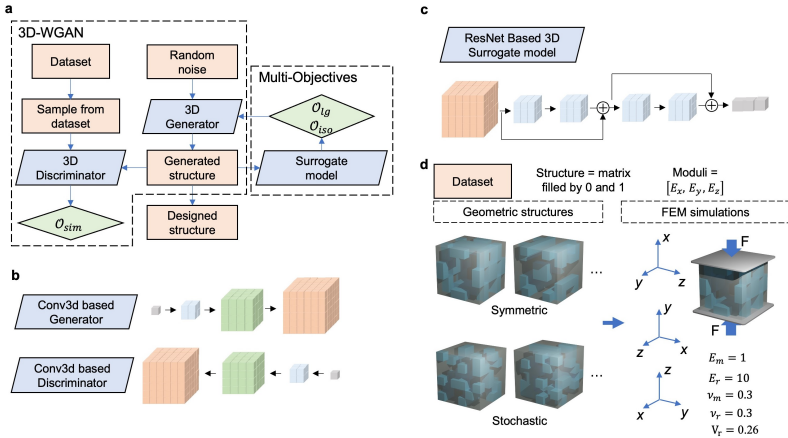


Fig. 1 Schematic illustration of the framework for multi-objective generative design of 3D composite materials. **a.** Overall framework. It is mainly a GAN based model whose generator and discriminator are built by 3D convolutional neural networks instead of 2D ones. \mathcal{O}_{sim} is the objective of generating similar structures with the dataset. A pre-trained surrogate model is introduced to predict the moduli of output composite structures from the generator. \mathcal{O}_{lg} and \mathcal{O}_{iso} are the objectives introduced to control the moduli and isotropy, separately. **b.** Dataset construction. Voxel model of 20,000 stochastic and 20,000 center-symmetric composite structures are generated in a $6 \times 6 \times 6$ space. The blue voxels represent for the reinforcements and the grey voxels represent for the matrix. The volume fraction $V_r=0.26$, the Young's moduli and Poisson's ratios of the matrix and reinforcements E_m , E_r , ν_m and ν_r , are kept the same for all the structures. Single-axial compression simulations are performed to get the elastic response of the generated composite structures in x , y and z direction. The dataset is constructed of structure tensors and moduli vectors E_x , E_y and E_z of the composite structures. **c.** 3D Wasserstein GAN network for structure generation. 3D Transposed convolutions are used to generate new structures from random seed while 3D convolutions are used to discriminate the structures generated by traditional Wasserstein GAN loss \mathcal{L}_{sim}^G and the moduli and isotropy objective losses \mathcal{L}_{lg} and \mathcal{L}_{iso} . **d.** Network of the surrogate model. Resnet-18 based surrogate models are used provide predicted moduli and isotropy for losses \mathcal{L}_{lg} and \mathcal{L}_{iso} calculation. The dataset construction by geometry generation and FEM simulations.

which means that we encourage the 3D-based generator to generate structures with the same moduli in all directions. Similar to \mathcal{O}_{lg} , it offers a tendency to the optimization of the 3D-based Generator.

According to these objectives, we embodied those goals by the training losses. Those losses will gradually fine tune the 3D-based Generator during the training process.

For objective \mathcal{O}_{sim} , we need to construct two parts of loss \mathcal{L}_{sim}^D and \mathcal{L}_{sim}^G denoting the loss for 3D-based discriminator and 3D-based generator, respectively. We follow the discriminator loss \mathcal{L}_{sim}^D from WGAN-GP[50] for our

3D-based discriminator, i.e.,

$$\mathcal{L}_{sim}^D = D_w(\tilde{x}) - D_w(x) + \lambda(\|\nabla_{\tilde{x}} D_w(x)\|_2 - 1)^2, \quad (1)$$

where D_w is the 3D-based discriminator, \tilde{x} is the fake sample generated by 3D-based generator G , x is the real sample from our dataset, and λ is the gradient penalty coefficient.

Again, we take the generator loss \mathcal{L}_{sim}^G from WGAN-GP[50], i.e.,

$$\mathcal{L}_{sim}^G = -D_w(\tilde{x}), \quad (2)$$

As mentioned in Figure 1, we have designed multiple additional losses for different objectives. We construct the loss \mathcal{L}_{lg} for objective \mathcal{O}_{lg} as follows:

$$\mathcal{L}_{lg} = w_{lg} \cdot \frac{1}{B} \sum_{i=1}^B \|E_{goal} - S(\tilde{x}_i)\|_2^2, \quad (3)$$

where w_{lg} is a hyperparameter that denotes the weight of loss \mathcal{L}_{lg} , B is the batch size, E_{goal} is the modulus goal we set. S is the pretrained surrogate model and \tilde{x}_i is the i -th sample in the batch. Thus, $S(\tilde{x}_i)$ is the predicted modulus of a generated sample.

Also, we construct the loss \mathcal{L}_{iso} for isotropy objective \mathcal{O}_{iso} , which can be represented as follows:

$$\mathcal{L}_{iso} = w_{iso} \cdot \frac{1}{B} \sum_{i=1}^B \sum_{j,k \in \{X,Y,Z\}, j \neq k} (S_j(\tilde{x}_i) - S_k(\tilde{x}_i))^2, \quad (4)$$

where w_{iso} is a hyperparameter that denotes the weight of loss \mathcal{L}_{iso} and S_X, S_Y, S_Z denotes the calculated moduli of X, Y, Z direction.

3D surrogate model

As introduced previously, our MDWGAN model includes a special component - 3D Surrogate Model (Fig 1). Our 3D Surrogate Model is based on ResNet-18[51]. Different from its original version, we switch its 2D convolutional networks to 3D convolutional networks and modify its pooling layers. We pre-trained the model to high accuracy before incorporating it to our framework (See method). Our pre-trained surrogate model can estimate the moduli of a given structure more efficiently compared to FEM (see Figure S), which allows us to significantly reduce our training time.

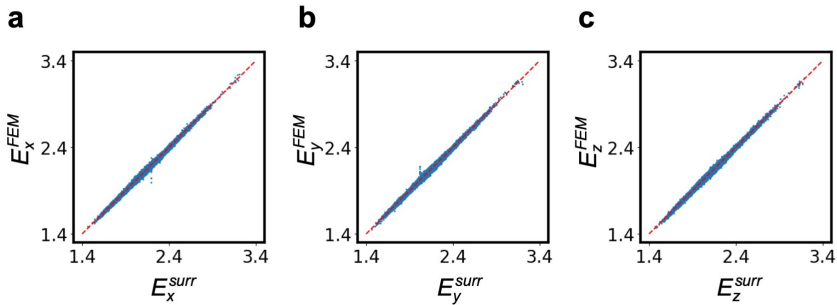


Fig. 2 Comparison between real moduli and moduli calculated by surrogate model on x, y and z axes.

Figure 2 gives us a view of calculated moduli versus real moduli. Based on our calculation, the variance of the real moduli is 3.63×10^{-2} , while the mean square error (MSE) between the moduli from our surrogate model and the real moduli is 2.02×10^{-4} . This result enables us to use the pre-trained 3D surrogate model to approximate the moduli of generated instance and accelerate the training process.

Database construction

To illustrate our framework, we generated multiple two-phase composite structures represented by representative volume elements (RVEs) filled with cubic voxels. Reinforcement volume fractions is set as $V_r = 0.26$. The Young's moduli and Poisson's ratio of the matrix and reinforcements E_m , E_r , ν_m and ν_r are kept the same across all the structures. The Young's moduli of the composite E_x , E_y and E_z are obtained (see Figure 1b and Methods). To test our framework's capability of quality generation with few feature and parameters, only the raw structure matrix representing the voxel model of the composites and their Young's moduli vectors are included, with no other extracted features, hyperparameters or constraints such as reinforcement volume fractions V_r or parameter of the structural symmetry and isotropy to support the model. To illustrate that our framework could generate composite structures with similar structural features, structures with both stochastic reinforcement distribution and central symmetric distributions (Figure 1b) are included. (As there are 230 crystallographic symmetry groups in 3D spaces, to exhaustively cover all the possible symmetries in our dataset is hard and not referential in practical research or industrial applications.) Without the consideration of symmetry, there are 2^{n^3} possible structures in an $n \times n \times n$ cubic voxel RVE. We select $n = 6$ in this work for easy distinguishable geometrical and structural features such as symmetry in generated structures.

Composite structures generation

To capture the structural features of the composites, our MDWGAN model with only \mathcal{O}_{sim} but no additional physics based objectives was first trained with random and symmetric dataset. The generated structures by trained model inference are shown in 3. It can be seen that the MDWGAN model

not only successfully produced structures with the reinforcement volume fraction around $V_r=0.26$, but also captured the geometrical symmetry information of the structures in our dataset (Figure 3a and b). Coefficient of asymmetry $C_{asymmetry}$ is introduced to evaluate the symmetry of the structure. We regard the fully central symmetric structures with $C_{asymmetry} = 0$, while the fully stochastic structures with $C_{asymmetry} = 1$ (See Method). The results show a clear difference between symmetric generations (less than 0.1, purple dots in Figure 3c) and random generations (large than 0.5, red dots in Figure 3c). Thus, structural features of the designs are successfully constrained by our dataset in terms of both V_r and $C_{asymmetry}$. As there are no additional objectives to control the properties involved, the distribution of the Young's moduli E_{avg} (Figure 3d and e) as well as the E_x , E_y and E_z (see Figure S1) of both symmetric and random structures generated are similar with those of the structures in our dataset. Similarly, the $C_{asymmetry}$ of the composite structures generated also follow the same distribution patterns with the training datasets (Figure 3f and g).

Multi-objective composite structures design

Based on the aforementioned \mathcal{O}_{sim} , \mathcal{O}_{lg} and \mathcal{O}_{iso} , we introduced multiple objectives based on the 3D WGAN model to control the average Young's moduli and the isotropy of the composite. Firstly, combining \mathcal{O}_{sim} and \mathcal{O}_{lg} by low, medium and high weights (see Methods), the stiffness of the structures are tuned while keeping similar symmetric and stochastic structural features. It can be seen from Figure 4a that the peak of distribution of the Young's moduli moves from left to right with the increase of the weight on \mathcal{O}_{lg} . As the design space of central symmetric structures for illustration are relatively limited (approximately 1.2×10^5), the structures with E_{avg} close to the upper limit are already in the training dataset. Thus, the distributions of the structures

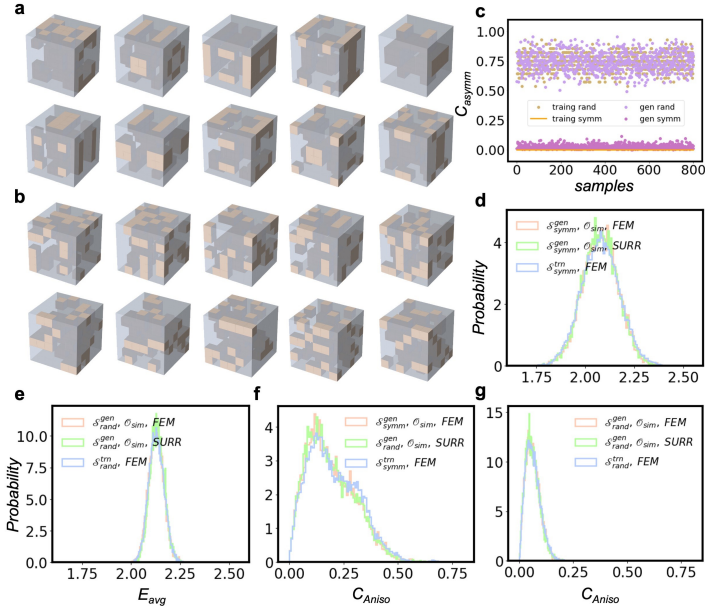


Fig. 3 The structures generated by MDWGAN without any additional objectives and restrictions. **a.** Generated random and symmetric composite structures. The light orange voxels represents for the reinforcements and the light blue voxels represents for the matrix. **b.** MDWGAN produces composite structures with volume fractions very close to $V_r=0.26$ set for the structures in training dataset. **c.** Symmetry evaluations of the structure. C_{asymm} the fully central symmetric structures with $C_{asymm} = 0$, while the fully stochastic structures with $C_{asymm} = 1$. **d.** The moduli E_x , E_y and E_z of the generated composite structures calculated by surrogate model and FEM.

generated under low, medium and high weight of \mathcal{O}_{lg}^{avg} narrows to the right side, with no significant increase in their largest value. On the contrary, the E_{avg} distributions of the structures generated overall shift to the right, with increased largest values, decreased smallest values and not largely changed width, because the feasible design region of stochastic structures are much larger (approximately 3.7×10^{51}). We also found that besides the E_{avg} , E_x , E_y and E_z are deviated from their distribution pattern of the training dataset as the bottom three violin plots of Figure 4b shows. It can be found in the generated structures of some trained models that the distributions of their E_x , E_y and E_z split apart, and the highest peak of E_x decreases while those of the E_y

and E_z increase (see also Figure S2). It could partly be attributed to the pattern differentiation of the generated structures. The plane-like reinforcement distributions and three dimensional symmetric distributions of the composite both occurs in the generated structures (see generated structures with largest moduli in Figure S3 - S8). It also can be seen that the average value of E_x decreases, while those of E_y and E_z increase slightly. Those might be caused by perturbations in training process. Obviously, by adding \mathcal{O}_{lg}^x objective, E_x could be enhanced (top two violin plots in Figure 4b). Although the generated structures achieve a E_{avg} enhancement, the volume fraction V_r and isotropic feature C_{aniso} of the generated structures doesn't change much (Figure 4c).

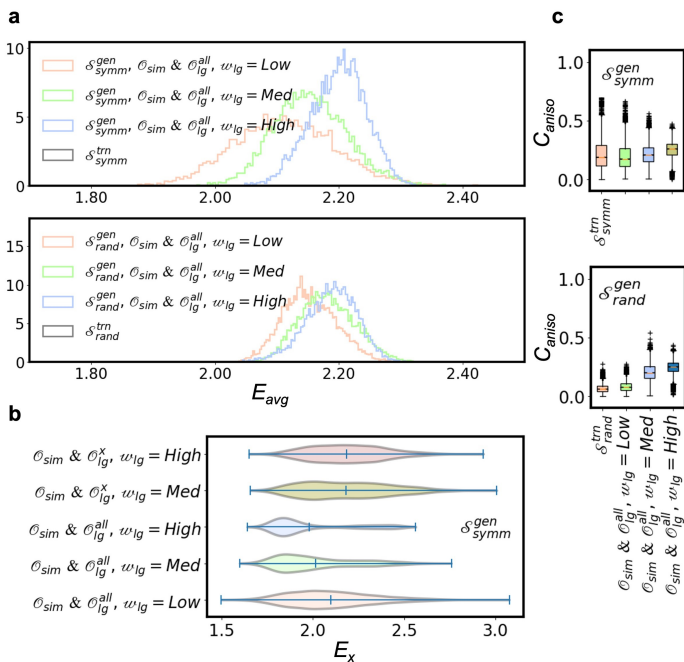


Fig. 4 The performance of model with $\mathcal{O}_{sim} + \mathcal{O}_{lg}$. **a.** Distributions of average moduli for generated samples and training dataset. δ_{symm}^{gen} denotes the moduli of generated samples of which the model has been trained on dataset with symmetrical samples. δ_{symm}^{trn} denotes the moduli of the symmetrical samples in the training dataset. **b.** Display of moduli on direction X for different generated samples. \mathcal{O}_{lg}^x means that enforcement for moduli on direction X is applied during the training. **c.** Box plot of anisotropic parameter C_{aniso} for different generated samples. C_{aniso} describes the anisotropic level for moduli of generated samples.

The isotropy of the composite is improved by adding \mathcal{O}_{iso} to the \mathcal{O}_{sim} objective (Figure 5a). From the statistical data of our generated symmetric structures, the C_{aniso} we defined (see Methods) can be remarkably reduced by rising the weight of \mathcal{O}_{iso} , while this effect is not noticeable on stochastic structure generations as stochastic structures are almost isotropic themselves (see Figure S9).

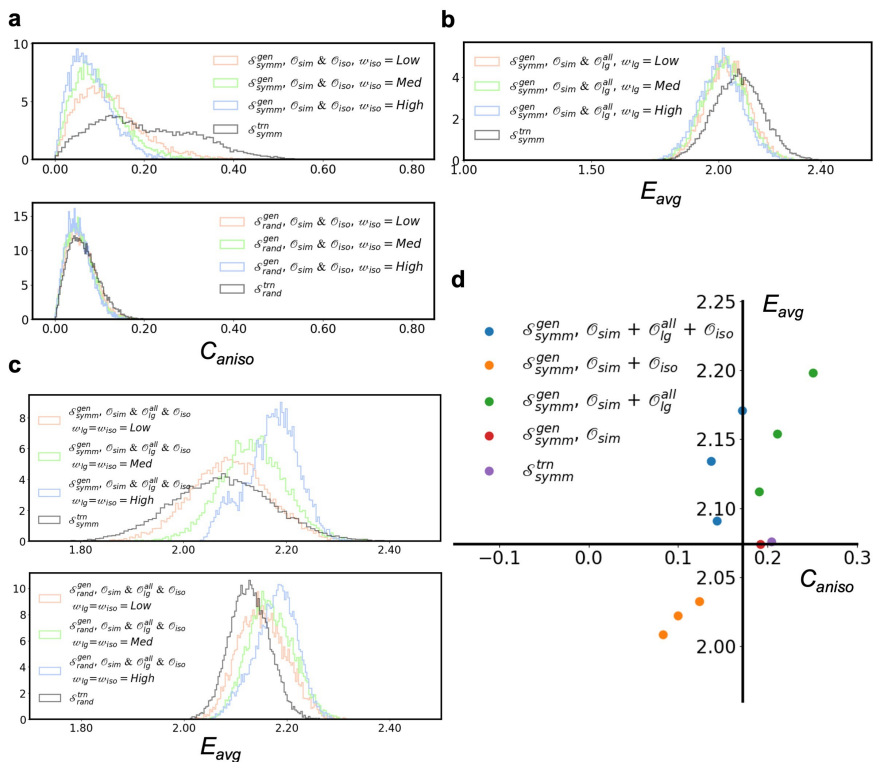


Fig. 5 The performance of model with $\mathcal{O}_{sim} + \mathcal{O}_{iso}$. **a.** Distributions of anisotropic parameter C_{aniso} for generated samples and training dataset. **b.** Distributions of average moduli for generated samples and training dataset.

We found that the E_{avg} of the structures generated under $\mathcal{O}_{sim} + \mathcal{O}_{iso}$ are marginally decreased (Figure 5b). Therefore, $\mathcal{O}_{sim} + \mathcal{O}_{lg} + \mathcal{O}_{iso}$ is used

reconcile this conflict-like effect (Figure 5d) and obtain composite structures with simultaneously higher Young's moduli and isotropy (Figure 5c).

Discussion

It is worth to check the correlations between E_{avg} , C_{Asymm} , C_{Aniso} of all the composite structures generated. As another common descriptor for composite structures, the connectivity [52, 53, 54], of both constituent phase are calculated (See Methods) and a coefficient of connectivity C_{Conne} is set as the largest number of connected components (voxels). According to the correlation heat map (Figure 6a), there are no convincing correlations between any of the two parameters on both symmetric and random (see Figure S10) composite structures generated. However, investigating the correlation scatter map of E_{avg} vs C_{Asymm} and E_{avg} vs C_{Aniso} , we could find that a higher weight of \mathcal{O}_{lg}^{all} statistically stimulates the generation of more asymmetric and anisotropic structures (Figure 6b and c). The reason may lie on that the objective \mathcal{O}_{lg}^{all} affects the objective \mathcal{O}_{sim} during training, which make the structural features of generated structures deviates from those of the dataset.

For the E_{avg} and C_{Conne} , we find they are, to some extent, related. We calculate the k-means cluster centers (see Method) on the scatter map between the E_{avg} and C_{Conne} of the 1% generated structure samples (here is 80 samples each for low, medium and high weight as we generated 8000 different structures under each weighted objective for the analysis). The k-cluster shows clear positive relates between E_{avg} and C_{Conne} in both symmetric and random structures generated. In the symmetric structures, two patterns of composites structures to enhance their Young's moduli are observed: to align the reinforcements in two axes (e.g., x and y) and to align the reinforcements in all three axes (x, y and z). When the weight of objective \mathcal{O}_{lg}^{all} is set as medium, the majority of

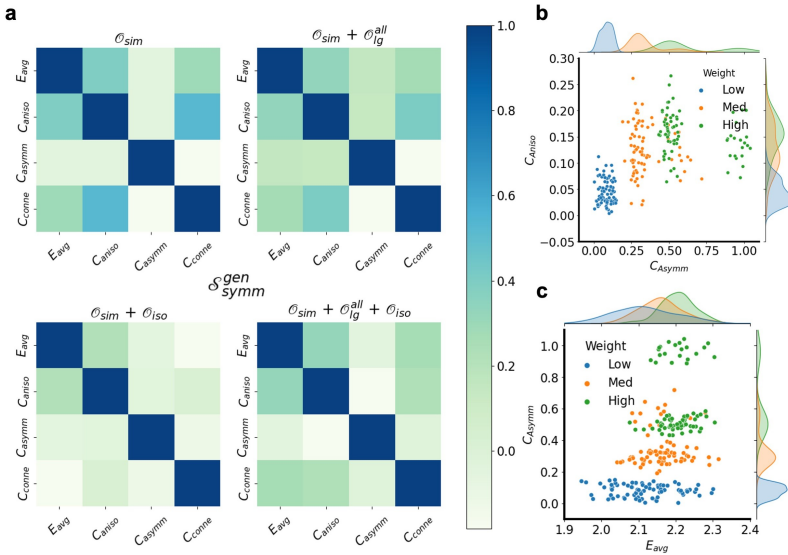


Fig. 6 Correlation between the features of generated symmetric structures. **a.** Heatmap of correlation between E_{avg} , C_{Asymm} , C_{Aniso} and C_{conne} . The shade degree of the color in each small square denotes the correlation between different parameters. Brunet squares means two parameters has high probability of correlation, both positive related or negative related. **b.** Scatter map of the correlation between C_{Asymm} and C_{Aniso} . **c.** Scatter map of the correlation between E_{avg} and C_{Asymm} .

the structures follows the two-axes alignment pattern of the reinforcements. The distribution peak of the maximum connected volume fraction of the reinforcement is around 0.13 (1/2 of V_r). However, when the weight of objective \mathcal{O}_{lg}^{all} goes to high, the three-axes alignment pattern takes the dominate position. The distribution peak of the maximum connected volume fraction of the reinforcement is close to $V_r = 0.26$. This also corresponds to the two different structural paradigms shown on the right side of Figure 7c (also see Figure S3 - S8).

The framework is capable of generating composite structures with similar, or even slightly larger Young's modulus than commonly regarded high stiffness structures (Figure 7e and f). For complex problems such as E_{avg} , the framework is capable of achieving the same or even better result than a robust topology optimization algorithm [55] (Figure 7e and g). Knowing that

the topology optimization methods work on mathematical models with clear definitions and expressions, the optimal solution is achieved by iteratively searching in the feasible region with optimal directions (see Method). Due to the complexity of the optimization model, one is likely to obtain several different optimized structures with different searching strategies. The performance of these optimized structures could be very close; thus they are regarded as the local optima in certain conditions. Therefore, each structure generated of proposed framework could also be considered as local optima in optimization space, but with large amount of samples, they are much closer to the global optima. It is also worth to mention that the FE evaluation of the modulus in topology optimization is slightly different from that in our framework in training and dataset construction. This may cause different optimization results. To systemically consider the advantages and disadvantages of our framework and topology optimization, and even integrate both to form a more effective and powerful tool for structure design should be a valuable direction for the future work.

Besides, it should be admitted that the dataset we constructed is more for framework illustration purpose. The selection or construction of a more well-developed, more informative material dataset should be of importance to demonstrate the full capability of this framework. Another future direction worth mentioning is to add active learning method into our training iterations for a more stable and mathematically complete framework.

In summary, we develop a 3D generative design framework for composite materials which consists of 3D WGAN, ResNet based surrogate, and multiple objectives of desired materials properties. It is demonstrated in this work that our MDWGAN framework successfully generates composite structures which are geometrically similar to those in our dataset (in terms of what is fixed such

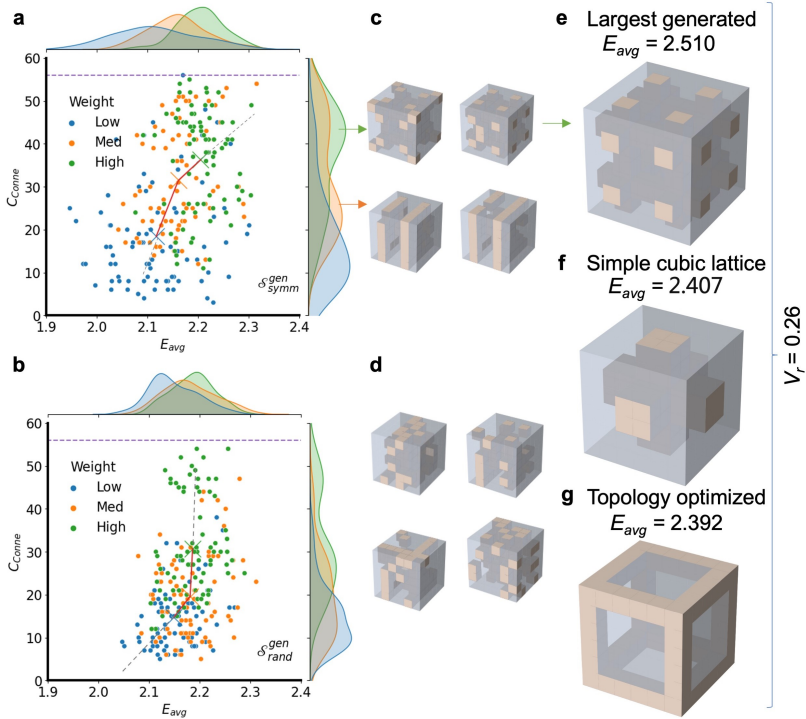


Fig. 7 Analysis of the design pattern for MDWGAN. Several typical samples are sampled from the peak of distribution wave. **a.** Scatter map with k-means cluster centers of low, medium and high weight of \mathcal{O}_{lg}^{all} of generated symmetric structure samples. **b.** Scatter map with k-means cluster centers of low, medium and high weight of \mathcal{O}_{lg}^{all} of generated random structure samples. **c.** Typical symmetric structures generated. **d.** Typical random structures generated. **e.** Structure generated with largest E_{avg} . **f.** Structure and E_{avg} of a common design, simple cubic lattice reinforced composite with same $V_r = 0.26$. **g.** Topology optimized structure and its E_{avg} with same $V_r = 0.26$.

as size, reinforcement volume fraction V_r and symmetry), but with tunable properties governed by multiple objectives. The properties of the composite in those objectives can be tuned by adjusting their weights. This framework could obviously be used to design single-phase architected materials, or composites consist of more than two phases with very minor adjustment. By changing the physics based objectives, the control and tune of the thermal, electrical and other material properties can also be achieved. Moreover, there is great potential for this framework in designing more complicated material structures such

as complex structural materials, biomaterials, and energy storage materials with the input of proper datasets and a little tailoring of the framework.

Methods

Data generation

In this work, we represent composite structures by voxel models. Discrete number zeros and ones representing for the matrix and the reinforcements of the composites are put in the corresponding indices of 3D structure matrices as structure data points. The volume fraction of the reinforcement is set as $56/216 \approx 0.26$. 20000 random structures are generated by randomly locating reinforcements in the RVE. 20000 structures with central symmetric reinforcements are generated by randomly locating 7 reinforcement voxels in $3 \times 3 \times 3$ RVE and mirror the structure on x , y and z axes. For simplicity, the constituent materials are regarded as isotropic. The Young's moduli of the reinforcement materials E_r are normalized by the Young's moduli of the matrix E_m , namely $E_m = 1$ and $E_r/E_m = 10$. Numerical single-axial compression test via FEM are performed three times on x , y and z direction of each generated structure. The compression is controlled by displacement of each directions applied on the corresponding surfaces while the opposite ones are fixed on the same directions. The Poison's ratio used here are $\nu_m = \nu_r = 0.3$. The Young's moduli of the composite E_x , E_y and E_z obtained are placed into one by three vectors. The voxel tensors and their Young's moduli vectors compose the dataset.

Training methodology

Before training our key framework, we train the 3D surrogate model in advance. It follows the basic regression model training procedure, by utilizing

a loss function to regular the behaviour of model. MSE loss is applied as the loss function of 3D surrogate model training.

Our training methodology of the key framework follows the idea of WGAN-GP[50] and implements some modifications. For every training batch, we train 3D-based generator and 3D-based discriminator in a separate way.

For training of the 3D-based discriminator, we first initialize a random noise and pass the random noise to the frozen 3D-based generator. 3D-based generator generates a 'fake' composite structure by sampling high-dimensional noise from its latent space. Then the 3D-based discriminator outputs its judgement on the generated fake sample. Meanwhile, a real sample is also passed into the 3D-based discriminator. Loss is then composed by three parts: fake sample loss, real sample loss and gradient penalty, which is presented in Eq. 1.

As for the training of 3D-based Generator, its training route is more complex since we expect it to accomplish multiple objectives. Again, we sample a high-dimensional random noise and pass it to the 3D-based generator. The 3D-based generator outputs a fake sample and the frozen 3D-based discriminator judges the performance of the fake sample. Then as introduced in section 4, we have different loss combinations for different objectives. For the objective of simply imitating the dataset, we just apply the loss \mathcal{L}_{sim}^G , which is shown in Eq. 2. As mentioned in section 4, this loss perform as a soft constraint to limit fraction of the strong phase and the geometrical information of the structure. Meanwhile, based on the different sample data format, this loss ensures the pattern of our generated sample, like symmetric or random. If we select structure with larger moduli as our objective, we will formulate the generator loss as $\mathcal{L}_{sim}^G + \mathcal{L}_{lg}$, which corresponds to the objective $\mathcal{O}_{sim} + \mathcal{O}_{lg}$. For the objective that seeks to generate models with isometric moduli, we will formulate the generator loss as $\mathcal{L}_{sim}^G + \mathcal{L}_{iso}$. It is also practical to formulate the generator

loss in the form of $\mathcal{L}_{sim}^G + \mathcal{L}_{lg} + \mathcal{L}_{iso}$, of which the performance is demonstrated in the Results section.

To make the update direction more precise, we iterate the training procedure of 3D-based discriminator multiple times but that of 3D-based once in one training batch. This strategy ensures 3D-based discriminator to keep leadership in the adversarial procedure and guide the behaviour of the 3D-based generator.

Data processing

In this work, E_{avg} is the arithmetic mean of E_x , E_y , and E_z . C_{aniso} is gauged by the standard deviation of E_x , E_y and E_z . C_{asymm} is calculated by the average difference between the structure matrix M_s and its flipped values along x , y and z axes. Structural connectivity is performed by cc3d package [56] following 6-connected neighborhood method in 3D . K-means cluster centers are derived by clustering module of scikit-learn package following classic k-means algorithm [57].

Topological optimization

In this work, the density-based topology optimization method is employed as a comparative example. The SIMP approach (Solid Isotropic Material Penalization) [58] is applied to the FEM voxel model. The material properties of each element are modeled of a power-law with the so-call pseudo-density $\rho \in [0, 1]$. $\rho = 0$ or 1 represents the material is matrix or reinforcement, separately. The penalty factor p is chosen as $p=3$ to ensure a clear binarized 0 and 1 solution. After setting the Young's modulus E_{avg} , volume fraction as objective and constraint function, the optimization problem can be solved with the OC

(optimality criteria) method [59]. The whole optimization algorithm is realized based on a compact MATLAB code package [60].

References

- [1] Suraj Rawal. Metal-matrix composites for space applications. *Jom*, 53(4):14–17, 2001.
- [2] Sungmin Hong, Dalton Sycks, Hon Fai Chan, Shaoting Lin, Gabriel P. Lopez, Farshid Guilak, Kam W. Leong, and Xuanhe Zhao. 3D Printing of Highly Stretchable and Tough Hydrogels into Complex, Cellularized Structures. *Advanced Materials*, 27(27):4035–4040, 2015.
- [3] Vivian R. Feig, Helen Tran, Minah Lee, and Zhenan Bao. Mechanically tunable conductive interpenetrating network hydrogels that mimic the elastic moduli of biological tissue. *Nature Communications*, 9(1):1–9, 2018.
- [4] Xinzhi Wang, Yibo Zhang, Xue Zhang, Ting Liu, Yuan Hua Lin, Liangliang Li, Yang Shen, and Ce Wen Nan. Lithium-Salt-Rich PEO/Li0.3La0.557TiO3 Interpenetrating Composite Electrolyte with Three-Dimensional Ceramic Nano-Backbone for All-Solid-State Lithium-Ion Batteries. *ACS Applied Materials and Interfaces*, 10(29):24791–24798, 2018.
- [5] L. D. Wegner and L. J. Gibson. Mechanical behaviour of interpenetrating phase composites - II: A case study of a three-dimensionally printed material. *International Journal of Mechanical Sciences*, 42(5):943–964, 2000.
- [6] M. Frey, L. Schneider, K. Masania, T. Keplinger, and I. Burgert. Delignified Wood-Polymer Interpenetrating Composites Exceeding the Rule of Mixtures. *ACS Applied Materials and Interfaces*, 11(38):35305–35311, 2019.

- 2019.
- [7] Jiecai Han, Changqing Hong, Xinghong Zhang, and Baolin Wang. Thermal shock resistance of TiB₂-Cu interpenetrating phase composites. *Composites Science and Technology*, 65(11-12):1711–1718, 2005.
- [8] Chang Zhou, Yongxiao Zhou, Qiang Zhang, Qingyu Meng, Lianyu Zhang, Equo Kobayashi, and Gaohui Wu. Near-zero thermal expansion of ZrW₂O₈/Al-Si composites with three dimensional interpenetrating network structure. *Composites Part B: Engineering*, 211(February):108678, 2021.
- [9] Wei Huang, Mehdi Shishehbor, Nicolás Guarín-Zapata, Nathan D. Kirchofer, Jason Li, Luz Cruz, Taifeng Wang, Sanjit Bhowmick, Douglas Stauffer, Praveena Manimunda, Krassimir N. Bozhilov, Roy Caldwell, Pablo Zavattieri, and David Kisailus. A natural impact-resistant bicontinuous composite nanoparticle coating. *Nature Materials*, 19(11):1236–1243, 2020.
- [10] Tiantian Li, Yanyu Chen, and Lifeng Wang. Enhanced fracture toughness in architected interpenetrating phase composites by 3D printing. *Composites Science and Technology*, 167(March):251–259, 2018.
- [11] Manuel E. Umanzor, Romesh C. Batra, Christopher B. Williams, and Alan P. Druschitz. Penetration Resistance of Cast Metal-Ceramic Composite Lattice Structures. *Advanced Engineering Materials*, 23(12):1–13, 2021.
- [12] T. A. Schaedler, A. J. Jacobsen, A. Torrents, A. E. Sorensen, J. Lian, J. R. Greer, L. Valdevit, and W. B. Carter. Ultralight metallic microlattices. *Science*, 334(6058):962–965, 2011.
- [13] Minh Son Pham, Chen Liu, Iain Todd, and Jedsada Lertthanasarn. Damage-tolerant architected materials inspired by crystal microstructure.

- Nature*, 565(7739):305–311, 2019.
- [14] Xu Chen, Yanlong Wu, Huilong Liu, Yaning Wang, Guangbin Zhao, Qingxian Zhang, Fu Wang, and Yaxiong Liu. Mechanical performance of PEEK-Ti6Al4V interpenetrating phase composites fabricated by powder bed fusion and vacuum infiltration targeting large and load-bearing implants. *Materials and Design*, 215:110531, 2022.
- [15] 3D Printing of Highly Stretchable and Tough Hydrogels into Complex, Cellularized Structures. *Advanced Materials*, 27(27):4035–4040, 2015.
- [16] Mingyang Zhang, Qin Yu, Zengqian Liu, Jian Zhang, Guoqi Tan, Da Jiao, Wenjun Zhu, Shujun Li, Zhefeng Zhang, Rui Yang, and Robert O. Ritchie. 3D printed Mg-NiTi interpenetrating-phase composites with high strength, damping capacity, and energy absorption efficiency. *Science Advances*, 6(19):1–10, 2020.
- [17] L. L. Hu, M. Zh Zhou, and H. Deng. Dynamic indentation of auxetic and non-auxetic honeycombs under large deformation. *Composite Structures*, 207(September 2018):323–330, 2019.
- [18] L. L. Hu, M. Zh Zhou, and H. Deng. Dynamic indentation of auxetic and non-auxetic honeycombs under large deformation. *Composite Structures*, 207(September 2018):323–330, 2019.
- [19] Mohamed Abdelhamid and Aleksander Czekanski. Impact of the lattice angle on the effective properties of the octet-truss lattice structure. *Journal of Engineering Materials and Technology, Transactions of the ASME*, 140(4):1747–1769, 2018.
- [20] Mark Helou, Sami Kara, Mark Helou, and Sami Kara. Design , analysis and manufacturing of lattice structures : an overview. *International Journal of Computer Integrated Manufacturing*, 31(3):243–261, 2018.
- [21] Tiantian Li, Yanyu Chen, Xiaoyi Hu, Yangbo Li, and Lifeng Wang.

24 REFERENCES

- Exploiting negative Poisson's ratio to design 3D-printed composites with enhanced mechanical properties. *Materials and Design*, 142:247–258, 2018.
- [22] L. Zhang, S. P. Lake, V. H. Barocas, M. S. Shephard, and R. C. Picu. Cross-linked fiber network embedded in an elastic matrix. *Soft Matter*, 9(28):6398–6405, 2013.
- [23] The elastic properties of composites reinforced by a transversely isotropic random fibre-network. *Composite Structures*, 208(August 2018):33–44, 2019.
- [24] Diab W. Abueidda, Ahmed S. Dalaq, Rashid K. Abu Al-Rub, and Iwona Jasiuk. Micromechanical finite element predictions of a reduced coefficient of thermal expansion for 3D periodic architected interpenetrating phase composites. *Composite Structures*, 133:85–97, 2015.
- [25] Diab W. Abueidda, Rashid K. Abu Al-Rub, Ahmed S. Dalaq, Dong Wook Lee, Kamran A. Khan, and Iwona Jasiuk. Effective conductivities and elastic moduli of novel foams with triply periodic minimal surfaces. *Mechanics of Materials*, 95:102–115, 2016.
- [26] Oraib Al-Ketan, Rashid K. Abu Al-Rub, and Reza Rowshan. Mechanical Properties of a New Type of Architected Interpenetrating Phase Composite Materials. *Advanced Materials Technologies*, 2(2):1600235, 2017.
- [27] Oraib Al-Ketan, Mhd Adel, Rashid K Abu Al-rub, Mhd Adel Assad, and Rashid K. Abu Al-Rub. Mechanical properties of periodic interpenetrating phase composites with novel architected microstructures. *Composite Structures*, 176:9–19, 2017.
- [28] Yunfei Zhang, Meng-Ting Hsieh, and Lorenzo Valdevit. Mechanical Performance of 3D Printed Interpenetrating Phase Composites with Spinodal

- Topologies. *Composite Structures*, 263(August 2020):113693, 2021.
- [29] Ahmet Cecen, Hanjun Dai, Yuksel C. Yabansu, Surya R. Kalidindi, and Le Song. Material structure-property linkages using three-dimensional convolutional neural networks. *Acta Materialia*, 146:76–84, 2018.
- [30] Tianju Xue, Thomas J. Wallin, Yigit Menguc, Sigrid Adriaenssens, and Maurizio Chiaramonte. Machine learning generative models for automatic design of multi-material 3D printed composite solids. *Extreme Mechanics Letters*, 41:100992, 2020.
- [31] Ruoqian Liu, Yuksel C. Yabansu, Ankit Agrawal, Surya R. Kalidindi, and Alok N. Choudhary. Machine learning approaches for elastic localization linkages in high-contrast composite materials. *Integrating Materials and Manufacturing Innovation*, 4(1):192–208, 2015.
- [32] Ruoqian Liu, Yuksel C. Yabansu, Zijiang Yang, Alok N. Choudhary, Surya R. Kalidindi, and Ankit Agrawal. Context Aware Machine Learning Approaches for Modeling Elastic Localization in Three-Dimensional Composite Microstructures. *Integrating Materials and Manufacturing Innovation*, 6(2):160–171, 2017.
- [33] Zijiang Yang, Yuksel C Yabansu, Reda Al-bahrani, Wei-keng Liao, and Alok N Choudhary. Deep learning approaches for mining structure-property linkages in high contrast composites from simulation datasets. *Computational Materials Science*, 151(December 2017):278–287, 2018.
- [34] Marat I. Latypov and Surya R. Kalidindi. Data-driven reduced order models for effective yield strength and partitioning of strain in multiphase materials. *Journal of Computational Physics*, 346:242–261, 2017.
- [35] Designing exceptional gas-separation polymer membranes using machine learning. *Science Advances*, 6(20):1–8, 2020.

- [36] Cheng Wen, Yan Zhang, Changxin Wang, Dezhen Xue, Yang Bai, Stoichko Antonov, Lanhong Dai, Turab Lookman, and Yanjing Su. Machine learning assisted design of high entropy alloys with desired property. *Acta Materialia*, 170:109–117, 2019.
- [37] Ankit Roy, Tomas Babuska, Brandon Krick, and Ganesh Balasubramanian. Machine learned feature identification for predicting phase and Young’s modulus of low-, medium- and high-entropy alloys. *Scripta Materialia*, 185:152–158, 2020.
- [38] Yanming Wang, Tian Xie, Arthur France-Lanord, Arthur Berkley, Jeremiah A. Johnson, Yang Shao-Horn, and Jeffrey C. Grossman. Toward Designing Highly Conductive Polymer Electrolytes by Machine Learning Assisted Coarse-Grained Molecular Dynamics. *Chemistry of Materials*, 32(10):4144–4151, 2020.
- [39] Grace X. Gu, Chun-Teh Chen, and Markus J. Buehler. De novo composite design based on machine learning algorithm. *Extreme Mechanics Letters*, 18:19–28, 2018.
- [40] Han Wei, Shuaishuai Zhao, Qingyuan Rong, and Hua Bao. Predicting the effective thermal conductivities of composite materials and porous media by machine learning methods. *International Journal of Heat and Mass Transfer*, 127:908–916, 2018.
- [41] Ziyuan Rao, PoYen Tung, Ruiwen Xie, Ye Wei, Hongbin Zhang, Alberto Ferrari, T. P. C. Klaver, Fritz Körmann, Prithiv Thoudden Sukumar, Alisson Kwiatkowski da Silva, Yao Chen, Zhiming Li, Dirk Ponge, Jörg Neugebauer, Oliver Gutfleisch, Stefan Bauer, and Dierk Raabe. Machine learning-enabled high-entropy alloy discovery. *Science*, 85(October):78–85, 2022.
- [42] K. T. Schütt, P. J. Kindermans, H. E. Saucedo, S. Chmiela,

- A. Tkatchenko, and K. R. Müller. SchNet: A continuous-filter convolutional neural network for modeling quantum interactions. *Advances in Neural Information Processing Systems*, 2017-December(1):992–1002, 2017.
- [43] Kristof T. Schütt, Farhad Arbabzadah, Stefan Chmiela, Klaus R. Müller, and Alexandre Tkatchenko. Quantum-chemical insights from deep tensor neural networks. *Nature Communications*, 8:6–13, 2017.
- [44] Niklas Gebauer, Michael Gastegger, and Kristof Schütt. Symmetry-adapted generation of 3d point sets for the targeted discovery of molecules. In H. Wallach, H. Larochelle, A. Beygelzimer, F. d'Alché-Buc, E. Fox, and R. Garnett, editors, *Advances in Neural Information Processing Systems 32*, pages 7566–7578. Curran Associates, Inc., 2019.
- [45] Niklas W. A. Gebauer, Michael Gastegger, Stefaan S. P. Hessmann, Klaus-Robert Müller, and Kristof T. Schütt. Inverse design of 3d molecular structures with conditional generative neural networks. *Nature Communications*, 13(1):1–11, 2022.
- [46] Juhwan Noh, Jaehoon Kim, Helge S. Stein, Benjamin Sanchez-Lengeling, John M. Gregoire, Alan Aspuru-Guzik, and Yousung Jung. Inverse Design of Solid-State Materials via a Continuous Representation. *Matter*, 1(5):1370–1384, 2019.
- [47] Yunwei Mao, Qi He, and Xuanhe Zhao. Designing complex architected materials with generative adversarial networks. *Science Advances*, 6(17), 2020.
- [48] Steve Kench and Samuel J. Cooper. Generating 3D structures from a 2D slice with GAN-based dimensionality expansion. *Nature Machine Intelligence*, 3:299–305, 2021.
- [49] Martin Arjovsky, Soumith Chintala, and Léon Bottou. Wasserstein

- GAN. In *ICML*, 2017.
- [50] Ishaan Gulrajani, Faruk Ahmed, Martín Arjovsky, Vincent Dumoulin, and Aaron C. Courville. Improved training of wasserstein gans. *CoRR*, abs/1704.00028, 2017.
- [51] Kaiming He, Xiangyu Zhang, Shaoqing Ren, and Jian Sun. Deep residual learning for image recognition. *CoRR*, abs/1512.03385, 2015.
- [52] Sen Lin, Nengzhuo Chou, Yujia Zhao, Yangfan Qin, Hao Jiang, Junjia Cui, Guangyao Li, and Yi Min Xie. Topological optimization of magnetic pulse welding coils with a connectivity-constrained particle swarm optimization algorithm. *Materials and Design*, 224:111337, 2022.
- [53] Stylianos Kechagias, Reece N. Oosterbeek, Maxwell J. Munford, Shaaz Ghose, and Jonathan R.T. Jeffers. Controlling the mechanical behaviour of stochastic lattice structures: The key role of nodal connectivity. *Additive Manufacturing*, 54(March):102730, 2022.
- [54] Mujan N. Seif, Dorothy J. Richardson, Katherine M. Moody, Mary Martin, Matthew Turner, Skylar W. Mays, T. John Balk, and Matthew J. Beck. Stochastic approach for determining properties of randomly structured materials: Effects of network connectivity. *Acta Materialia*, 222, 2022.
- [55] Ole Sigmund and Kurt Maute. Topology optimization approaches. *Structural and Multidisciplinary Optimization*, 48:1031–1055, 12 2013.
- [56] Silliam Silversmith. Connected components 3d 3.10.3. <https://github.com/seung-lab/connected-com>, 2022.
- [57] F. Pedregosa, G. Varoquaux, A. Gramfort, V. Michel, B. Thirion, O. Grisel, M. Blondel, P. Prettenhofer, R. Weiss, V. Dubourg, J. Vanderplas, A. Passos, D. Cournapeau, M. Brucher, M. Perrot, and E. Duchesnay. Scikit-learn: Machine learning in Python. *Journal of Machine*

- Learning Research*, 12:2825–2830, 2011.
- [58] M. P. Bendsøe and O. Sigmund. Material interpolation schemes in topology optimization. *Archive of Applied Mechanics (Ingenieur Archiv)*, 69:635–654, 11 1999.
- [59] Martin P. Bendsøe. *Optimization of Structural Topology, Shape, and Material*. Springer Berlin Heidelberg, 1995.
- [60] O. Sigmund. A 99 line topology optimization code written in matlab. *Structural and Multidisciplinary Optimization*, 21:120–127, 4 2001.